low dielectric constant solvents, ion pairing reduces the strength of solvation and the counterion displaces solvent, thus decreasing the solvent contribution. The variation in the solvent contribution can apparently overcome other contributions and even change the sign of ΔV^*.

Acknowledgment. We are pleased to acknowledge financial support from the National Science Foundation for this work.

Supplementary Material Available: Tables 1–25, listing rate constants as a function of temperature, pressure, solvent, and reactant (13 pages). Ordering information is given on any current masthead page.

Contribution from the Department of Chemistry and Laboratory for Molecular Structure and Bonding, Texas A&M University, College Station, Texas 77843

Compounds Containing Linked, Multiply-Bonded Dimetal Units. 1. Tetrakis(μ-6-chloro-2-hydroxypyridinato)diruthenium(II,III) Cations Linked Axially by Pyrazine. Comparison with a Single Molecule Axially Coordinated by Pyridine

F. Albert Cotton,* Youngmee Kim, and Tong Ren

Received December 2, 1991

The tetranuclear compound $[\{Ru_2(chp)_4\}_2(pyz)](BF_4)_2$ and the dinuclear compound $[Ru_2(chp)_4(py)](BF_4)$ were prepared by substitution of an axial chloride ligand of $Ru_2(chp)_4Cl$ with pyrazine and pyridine, respectively. Each compound has been characterized by X-ray crystallography and by magnetic susceptibility measurements from ca. 5 to ca. 300 K. $[\{Ru_2(chp)_4\}_2(pyz)](BF_4)_2$ crystallizes with four solvent molecules in space group $P2_1/c$ (No. 14). With $(CH_2Cl_2)_2$ and $(pyz)_2$ the unit cell has $a = 12.414$ (3) Å, $b = 16.083$ (5) Å, $c = 17.812$ (4) Å, $\beta = 97.915$ (2)°, $V = 3522$ (2) Å, and $Z = 2$. With $(CH_2Cl_2)_4$, the very similar unit cell has $a = 12.081$ (4) Å, $b = 16.469$ (4) Å, $c = 17.209$ (3) Å, $\beta = 98.28$ (2)°, $V = 3390$ (2) Å^3, and $Z = 2$. $[Ru_2(chp)_4(py)](BF_4)$ crystallizes in a triclinic cell with $a = 13.907$ (3) Å, $b = 16.322$ (3) Å, $c = 9.168$ (1) Å, $\alpha = 106.09$ (1)°, $\beta = 99.89$ (2)°, $\gamma = 76.88$ (2)°, $V = 1934$ (1) Å^3, and $Z = 2$. The pyrazine ligand bridges two diruthenium species in the $[\{Ru_2(chp)_4\}_2(pyz)]^{2+}$ cation, and the pyridine ligand coordinates to one axial position in the $[Ru_2(chp)_4(py)]^+$ ion. The pyridine or pyrazine nitrogen atoms are in all cases attached to the ruthenium atoms that are coordinated by oxygen atoms. The two complexes show similar magnetic behavior; they exhibit Curie–Weiss behavior, and the decrease in moment at low temperatures results primarily from zero-field splitting effects. There is no significant magnetic exchange interaction between the two dinuclear species in the $[\{Ru_2(chp)_4\}_2(pyz)]^{2+}$ ion.

Introduction

The work to be reported in the series of papers of which this is the first lies at the intersection of two lines of study. The electronic interactions, especially magnetic interactions, between paramagnetic transition metal atoms linked by bridging groups is an old and heavily explored field[1] although still full of challenging problems. On the other hand there has recently been emerging a new research thrust concerning the synthesis of oligomers and polymers that consists of multiply-bonded dimetal units linked together, in various ways, by shared bi- and multidentate ligands.[2]

The dinuclear multiply-bonded compounds of ruthenium and osmium have been extensively investigated in this laboratory in recent years, and we have been able to clarify their electronic structures quite considerably. The main species are built on Ru_2^{4+}, Ru_2^{5+}, and Os_2^{6+} cores, all of which display full or partial paramagnetism. Moreover, this paramagnetism arises, in whole or in part, from the presence of unpaired electrons in M–M π^* orbitals. It should therefore be possible, at least in principle, to build interactive pathways between such M_2 cores by connecting them, through their axial positions, by bridging ligands that have π systems of their own. That, in summary, is the concept that we shall be trying to implement in the work to be reported in this series of papers.

We begin here with very simple questions: (1) If we take two molecules that contain Ru_2^{5+} cores in their quartet ground states based on the $\sigma^2\pi^4\delta^2\pi^{*2}\delta^*$ configuration, can we couple them by some bidentate ligand that has a π system? (2) If we do so, will there be a detectable magnetic coupling of some kind between the linked Ru_2^{5+} cores?

In our first effort to address these questions we have chosen the tetrakis(μ-6-chloro-2-hydroxypyridinato)diruthenium(II,III) cation[3] (as its BF_4^- salt) and employed pyrazine, 1,4-diazabenzene, as the linking ligand, since this molecule has previously been used successfully in other systems.[4-9] To have a standard for the behavior of an individual molecule with as similar a set of ligands as possible, we have also prepared and studied the same Ru_2^{5+} complex containing pyridine as the axial ligand.

Experimental Section

The starting material, $Ru_2(chp)_4Cl$, was prepared by using a literature procedure.[3] $Ag(CH_3CN)_4BF_4$ was prepared by addition of acetonitrile to $AgBF_4$.

Preparation of $[\{Ru_2(chp)_4\}_2(pyz)](BF_4)_2$ (1). A 0.25-g (0.33-mmol) sample of $Ru_2(chp)_4Cl$ and 0.21 g (0.66 mmol) of $Ag(CH_3CN)_4BF_4$ were dissolved in 20 mL of dichloromethane and stirred overnight under argon. A white precipitate of AgCl and some unreacted $AgBF_4$ were removed by filtration. Evaporation of the filtrate provided $[Ru_2(chp)_4(CH_3CN)](BF_4)$, which is very hygroscopic. This intermediate was dissolved in 20 mL of CH_2Cl_2, and pyrazine, 0.053 g (0.66 mmol), was added. This solution was heated to reflux for 2 h and cooled, and hexane was added to precipitate a dark purple solid. Yields were typically 0.25–0.30 g (ca. 50%). IR (KBr, cm^{-1}): 3100 w, 1594 s, 1527 s, 1437 s, 1388 m, 1339 s, 1225 w, 1172 s, 1054 s, 1015 s, 934 m, 876 s, 792 s, 722 s, 630 s. Crystalline material suitable for X-ray work and magnetic study was obtained by slow diffusion of hexane into a portion of the CH_2Cl_2 solution. The solvent content of the crystals varies, in a way which we do not understand. In one case we obtained **1**·$4CH_2Cl_2$. For further details see below under X-ray crystallography.

Preparation of $[Ru_2(chp)_4(py)](BF_4)$·hexane·py (2). A 50-mL volume of pyridine was added to $[Ru_2(chp)_4(CH_3CN)](BF_4)$ instead of pyrazine in a similar procedure, and the reaction mixture was stirred overnight.

---

(1) Willet, R. D., Gatteschi, D., Kahn, O., Eds. *Magneto-Structural Correlations in Exchange Coupled Systems*; Reidel: Dordrecht, Holland, 1985.

(2) (a) Kerby, M. C.; Eichhorn, B. W.; Creighton, J. A.; Vollhardt, K. P. C. *Inorg. Chem.* **1990**, *29*, 1319. (b) Cayton, R. H.; Chisholm, M. H.; Huffman, J. C.; Lobkovsky, E. B. *J. Am. Chem. Soc.* **1991**, *113*, 8709.

(3) Chakravarty, A. R.; Cotton, F. A.; Tocher, D. A. *Inorg. Chem.* **1985**, *24*, 1263.

(4) Real, J. A.; De Munno, G.; Munoz, M. C.; Julve, M. *Inorg. Chem.* **1991**, *30*, 2701.

(5) Carreck, P. W.; Goldstein, M.; McPartlin, E. M.; Unworth, W. D. *J. Chem. Soc., Chem. Commun.* **1991**, 1634.

(6) Richardson, H. W.; Hatfield, W. E. *J. Am. Chem. Soc.* **1976**, *98*, 835.

(7) Santoro, A.; Mighell, A. D.; Reimann, C. W. *Acta Crystallogr., Sect. B* **1970**, *B26*, 979.

(8) Darriet, J.; Haddad, M. S.; Duester, E. N.; Hendrickson, D. N. *Inorg. Chem.* **1979**, *18*, 2679.

(9) Morosin, B.; Hughes, R. C.; Soos, Z. G. *Acta Crystallogr., Sect. B* **1975**, *B31*, 762.

0020-1669/92/1331-2608$03.00/0

Table I. Crystallographic Data for $[\{Ru_2(chp)_4\}_2(pyz)](BF_4)_2\cdot 4CH_2Cl_2$ and $[Ru_2(chp)_4(py)](BF_4)\cdot$hexane$\cdot$py

	$[\{Ru_2(chp)_4\}_2(pyz)]$-$(BF_4)_2\cdot 4CH_2Cl_2$	$[Ru_2(chp)_4(py)]$-$(BF_4)\cdot$hexane$\cdot$py
formula	$Ru_4Cl_{16}O_8N_{10}C_{48}$-$B_2F_8H_{36}$	$Ru_2Cl_4O_4N_6C_{36}$-BF_4H_{36}
fw	1686.3	865.07
space group	$P2_1/c$ (No. 14)	$P\bar{1}$ (No. 2)
a, Å	12.081 (4)	13.907 (3)
b, Å	16.469 (4)	16.322 (3)
c, Å	17.209 (3)	9.168 (1)
α, deg	90.00 (0)	106.09 (1)
β, deg	98.28 (2)	99.89 (2)
γ, deg	90.00 (0)	76.88 (2)
V, $Å^3$	3390 (2)	1934 (1)
Z	2	2
d_{calc}, g/cm^3	1.652	1.488
cryst size, mm	0.20 × 0.35 × 0.45	0.30 × 0.18 × 0.15
μ, cm^{-1}	12.467	95.895
data collcn instrument	Enraf-Nonius CAD-4	AFC5R Rigaku
radiation monochromated in incident beam, Å	0.71073	1.540598
orientation reflcns: no.; range (2θ), deg	25; $20.34 < 2\theta \leq 28.56$	18; $43.6 < 2\theta \leq 47.18$
temp, °C	−100	20
scan method	ω	2θ–ω
data collcn range (2θ), deg	$4 \leq 2\theta \leq 50$	$4 \leq 2\theta \leq 115$
no. of unique data; tot. no. with $F_o^2 > 3\sigma(F_o^2)$	6183; 5112	5555; 4568
no. of params refined	433	421
transm factors: max; min	1.00; 0.89	1.00; 0.73
R^a	0.053	0.058
R_w^b	0.076	0.085
quality-of-fit indicator[c]	2.426	2.109
largest shift/esd, final cycle	0.03	0.673
largest peak, e/$Å^3$	1.585	0.992

[a] $R = \sum||F_o| - |F_c||/\sum|F_o|$. [b] $R_w = [\sum w(|F_o| - |F_c|)^2/\sum w|F_o|^2]^{1/2}$; $w = 1/\sigma^2(|F_o|)$. [c] Quality-of-fit $= [\sum w(|F_o| - |F_c|)^2/(N_{observns} - N_{params})]^{1/2}$.

Table II. Positional Parameters and *B* Values and Their Estimated Standard Deviations for $[\{Ru_2(chp)_4\}_2(pyz)](BF_4)_2\cdot 4CH_2Cl_2$

atom	*x*	*y*	*z*	B^a, $Å^2$
Ru(1)	0.21779 (4)	0.15486 (3)	0.03811 (3)	1.887 (9)
Ru(2)	0.35524 (4)	0.24930 (3)	0.05922 (3)	1.808 (9)
Cl(1)	0.4486 (1)	0.3744 (1)	0.2035 (1)	3.02 (3)
Cl(2)	0.3769 (2)	0.4472 (1)	0.0226 (1)	3.35 (4)
Cl(3)	0.5523 (2)	0.3175 (1)	−0.0404 (1)	3.65 (4)
Cl(4)	0.6181 (1)	0.2501 (1)	0.1384 (1)	3.72 (4)
O(1)	0.1145 (3)	0.2263 (3)	0.0862 (3)	2.36 (8)
O(2)	0.1630 (4)	0.2023 (3)	−0.0657 (3)	2.40 (9)
O(3)	0.3177 (4)	0.0798 (3)	−0.0097 (3)	2.40 (9)
O(4)	0.2676 (4)	0.1045 (3)	0.1422 (3)	2.54 (9)
N(1)	0.2650 (4)	0.3049 (3)	0.1394 (3)	1.99 (9)
N(2)	0.2652 (4)	0.3171 (3)	−0.0308 (3)	2.4 (1)
N(3)	0.4376 (4)	0.1865 (3)	−0.0213 (3)	2.2 (1)
N(4)	0.4318 (4)	0.1741 (3)	0.1483 (3)	2.4 (1)
N(5)	0.0790 (4)	0.0608 (3)	0.0155 (3)	2.1 (1)
C(1)	0.0714 (5)	0.0004 (4)	0.0661 (4)	2.5 (1)
C(2)	0.0078 (5)	0.0592 (4)	−0.0514 (4)	2.5 (1)
C(11)	0.1549 (5)	0.2852 (4)	0.1348 (4)	2.5 (1)
C(12)	0.0843 (6)	0.3261 (4)	0.1795 (4)	2.8 (1)
C(13)	0.1291 (6)	0.3829 (5)	0.2321 (4)	3.3 (2)
C(14)	0.2454 (6)	0.4008 (4)	0.2410 (4)	3.0 (1)
C(15)	0.3063 (5)	0.3590 (4)	0.1943 (4)	2.4 (1)
C(21)	0.1863 (5)	0.2779 (4)	−0.0814 (4)	2.5 (1)
C(22)	0.1281 (6)	0.3161 (4)	−0.1469 (4)	3.3 (1)
C(23)	0.1487 (7)	0.3971 (5)	−0.1604 (5)	4.1 (2)
C(24)	0.2276 (6)	0.4399 (5)	−0.1084 (4)	3.4 (1)
C(25)	0.2814 (5)	0.3978 (4)	−0.0460 (4)	2.7 (1)
C(31)	0.4058 (5)	0.1073 (4)	−0.0366 (4)	2.4 (1)
C(32)	0.4681 (6)	0.0565 (4)	−0.0801 (4)	2.6 (1)
C(33)	0.5584 (6)	0.0874 (4)	−0.1090 (4)	2.9 (1)
C(34)	0.5869 (6)	0.1711 (5)	−0.0983 (4)	3.1 (1)
C(35)	0.5242 (5)	0.2146 (4)	−0.0549 (4)	2.5 (1)
C(41)	0.3680 (5)	0.1180 (4)	0.1778 (4)	2.4 (1)
C(42)	0.4094 (7)	0.0721 (4)	0.2458 (4)	3.3 (1)
C(43)	0.5194 (7)	0.0850 (5)	0.2795 (5)	3.9 (2)
C(44)	0.5872 (7)	0.1413 (5)	0.2484 (5)	3.7 (2)
C(45)	0.5394 (6)	0.1830 (4)	0.1826 (4)	3.2 (1)
B	0.1860 (7)	−0.1221 (5)	0.2589 (5)	3.0 (2)
F(1)	0.1118 (4)	−0.0592 (3)	0.2360 (3)	4.6 (1)
F(2)	0.1858 (4)	−0.1344 (3)	0.3380 (3)	4.3 (1)
F(3)	0.1504 (7)	−0.1927 (4)	0.2233 (4)	8.8 (2)
F(4)	0.2889 (4)	−0.1010 (3)	0.2450 (3)	6.0 (1)
C(46)	0.8715 (6)	0.1579 (5)	0.1276 (5)	3.9 (2)
Cl(5)	0.7799 (2)	0.0974 (2)	0.0618 (2)	6.46 (6)
Cl(6)	0.8923 (3)	0.1055 (2)	0.2184 (2)	8.16 (8)
C(47)	0.088 (2)	0.6130 (9)	0.0104 (8)	10.0 (5)
Cl(7)	0.1200 (3)	0.5352 (2)	0.0793 (2)	8.88 (9)
Cl(8)	0.1295 (3)	0.7079 (3)	0.0540 (3)	9.2 (1)

[a] *B* values for anisotropically refined atoms are given in the form of the isotropic equivalent displacement parameter defined as $(4/3)[a^2B(1,1) + b^2B(2,2) + c^2B(3,3) + ab(\cos\gamma)B(1,2) + ac(\cos\beta)B(1,3) + bc(\cos\alpha)B(2,3)]$.

The dark purple precipitate was collected by addition of hexane and dried under vacuum; yield 0.17 g (60%). IR (KBr, cm^{-1}): 3097 w, 1596 m, 1529 w, 1437 s, 1389 w, 1340 w, 1216 w, 1171 w, 1121 w, 1081 s, 1015 s, 931 w, 793 w, 720 w, 626 w. A crystal obtained by slow diffusion of hexane into a pyridine solution was used for the X-ray data collection.

Measurements. Solid-state (KBr disk) infrared spectra were recorded from 4000 to 600 cm^{-1} on a Perkin-Elmer 881 spectrophotometer. Magnetic susceptibility measurements were carried out in the 5–300 K temperature range with a SQUID (superconducting quantum interference device) at Northwestern University. The samples were all quenched in a field of 5 kG.

X-ray Crystallography. The determination of the crystal systems, data collection procedures, structure solutions, and refinements were all carried out by procedures that have been described before.[10,11] Lorentz, polarization, and absorption corrections[12] were always applied.

Compound **1** was first obtained as $\mathbf{1}\cdot 2CH_2Cl_2\cdot 2$pyz, and the structure was solved and refined. The crystals belonged to the monoclinic system, space group $P2_1/c$ with $a = 12.414$ (3) Å, $b = 16.083$ (5) Å, $c = 17.812$ (4) Å, $\beta = 97.915$ (2), $V = 3522$ (2) Å, and $Z = 2$. The refinement was not as satisfactory as we desired ($R = 0.075$, $R_w = 0.100$), and the BF_4^- ions were disordered. However, the pyrazine-bridged cation $[Ru_2(chp)_4(C_4H_4N_2)Ru_2(chp)_4]^{2+}$ was clearly defined and the dimensions were acceptable. Nevertheless, it was decided to recollect the X-ray data at lower temperature, on another crystal, from another preparation, in the hope of getting a more satisfactory refinement. To our surprise, this second crystal was not identical to the first one but instead had the composition $\mathbf{1}\cdot 4CH_2Cl_2$. The two crystals differ slightly in their unit cell dimensions and in the kinds, but not the number, of interstitial solvent molecules, but they are generally very similar, with essentially the same packing arrangement. One other feature of $\mathbf{1}\cdot 4CH_2Cl_2$ that was very welcome is that the BF_4^- ions show no disorder. Overall, the second structure is far better than the first one, and we therefore give the details of this second one only. However, all of the details concerning $\mathbf{1}\cdot 2CH_2Cl_2\cdot 2$pyz are available in the supplementary material.

A dark purple, block-shaped crystal of $\mathbf{1}\cdot 4CH_2Cl_2$ having dimensions 0.20 × 0.35 × 0.45 mm was mounted on a fiber. Data were collected on an Enraf-Nonius CAD-4 diffractometer equipped with graphite-monochromated Mo Kα (λ = 0.71073 Å) radiation at −100 °C. The unit cell was determined to be monoclinic on the basis of 25 reflections in the range $20° < 2\theta < 29°$. The data were collected by using the ω scan technique in the range $4° \leq 2\theta \leq 50°$. The overall decay of intensity during the period of data collection was only 1.7%. The space group was determined as $P2_1/c$ (No. 14) on the basis of the systematic absences. Crystallographic details are summarized in Table I.

The Patterson map revealed the positions of two ruthenium atoms; the positions of the other non-hydrogen atoms were obtained by an alternating sequence of difference Fourier maps and least-square refinements. All atoms were ultimately refined with anisotropic thermal parameters. The atomic positional parameters are given in Table II.

$[Ru_2(chp)_4(py)](BF_4)\cdot$hexane$\cdot$py. A dark purple block (0.30 × 0.18 × 0.15 mm) was mounted on a glass fiber with epoxy resin. A triclinic

---

(10) Bino, A.; Cotton, F. A.; Fanwick, P. E. *Inorg. Chem.* **1979**, *18*, 3558.
(11) Cotton, F. A.; Frenz, B. A.; Deganello, G.; Shaver, A. J. *Organomet. Chem.* **1973**, *50*, 227.
(12) North, A. C. T.; Phillips, D. C.; Mathews, F. S. *Acta Crystallogr., Sect. A: Cryst. Phys., Diffr., Theor. Gen. Crystallogr.* **1968**, *24A*, 351.

Table III. Positional Parameters and *B* Values and Their Estimated Standard Deviations for $[Ru_2(chp)_4(py)](BF_4)\cdot$hexane·py

atom	*x*	*y*	*z*	B,[a] Å^2
Ru(1)	0.30228 (4)	0.18941 (4)	0.19221 (7)	3.61 (2)
Ru(2)	0.20857 (5)	0.28332 (4)	0.37030 (7)	3.78 (2)
Cl(1)	0.4890 (2)	0.0189 (2)	0.2031 (3)	6.11 (7)
Cl(2)	0.5154 (2)	0.1879 (2)	0.0694 (3)	6.03 (7)
Cl(3)	0.3063 (2)	0.1664 (2)	−0.1820 (3)	5.78 (7)
Cl(4)	0.2852 (2)	−0.0004 (2)	−0.0500 (3)	6.05 (7)
O(1)	0.3273 (5)	0.2916 (4)	0.5230 (6)	4.9 (2)
O(2)	0.2290 (5)	0.3819 (4)	0.3032 (7)	4.9 (2)
O(3)	0.0865 (4)	0.2784 (4)	0.2232 (6)	4.4 (2)
O(4)	0.1837 (5)	0.1845 (4)	0.4372 (6)	4.6 (2)
N(1)	0.4119 (5)	0.1678 (5)	0.3741 (8)	4.4 (2)
N(2)	0.3577 (5)	0.2935 (5)	0.1776 (8)	4.2 (2)
N(3)	0.1844 (5)	0.2195 (4)	0.0286 (7)	3.8 (2)
N(4)	0.2385 (5)	0.0911 (4)	0.2170 (7)	4.0 (2)
N(5)	0.1165 (6)	0.3727 (5)	0.5436 (8)	4.8 (2)
C(1)	0.4899 (7)	0.1017 (6)	0.370 (1)	4.9 (3)
C(2)	0.5638 (8)	0.0930 (8)	0.481 (1)	6.5 (3)
C(3)	0.5607 (8)	0.1615 (9)	0.618 (1)	7.3 (4)
C(4)	0.4813 (8)	0.2287 (8)	0.630 (1)	6.2 (3)
C(5)	0.4054 (6)	0.2302 (6)	0.509 (1)	4.6 (3)
C(6)	0.4397 (7)	0.2899 (6)	0.108 (1)	5.1 (3)
C(7)	0.4648 (8)	0.3559 (7)	0.073 (1)	6.4 (3)
C(8)	0.4013 (9)	0.4370 (8)	0.109 (2)	7.4 (4)
C(9)	0.3201 (9)	0.4469 (7)	0.187 (1)	6.2 (3)
C(10)	0.3034 (6)	0.3740 (6)	0.222 (1)	4.6 (3)
C(11)	0.1886 (6)	0.2043 (6)	−0.1224 (9)	4.5 (2)
C(12)	0.1086 (7)	0.2195 (7)	−0.231 (1)	5.5 (3)
C(13)	0.0159 (8)	0.2510 (7)	−0.180 (1)	6.2 (3)
C(14)	0.0071 (7)	0.2699 (6)	−0.024 (1)	5.0 (3)
C(15)	0.0940 (6)	0.2548 (5)	0.0761 (9)	3.8 (2)
C(16)	0.2427 (7)	0.0115 (6)	0.122 (1)	5.0 (3)
C(17)	0.2187 (9)	−0.0586 (7)	0.152 (1)	6.3 (3)
C(18)	0.1796 (9)	−0.0435 (8)	0.292 (1)	7.1 (4)
C(19)	0.1713 (8)	0.0388 (7)	0.393 (1)	6.0 (3)
C(20)	0.1983 (7)	0.1053 (6)	0.3507 (9)	4.5 (3)
C(21)	0.0179 (7)	0.3784 (7)	0.526 (1)	5.8 (3)
C(22)	−0.0430 (8)	0.4368 (8)	0.637 (1)	7.0 (4)
C(23)	−0.001 (1)	0.4859 (9)	0.761 (2)	8.1 (4)
C(24)	0.103 (1)	0.4816 (9)	0.780 (1)	8.5 (4)
C(25)	0.1580 (8)	0.4246 (7)	0.670 (1)	6.5 (3)
B	0.273 (1)	0.667 (1)	0.107 (2)	9.1 (4)*
F(1a)	0.227 (1)	0.758 (1)	0.166 (2)	9.7 (4)*
F(2a)	0.293 (2)	0.614 (2)	−0.058 (3)	15.8 (8)*
F(3a)	0.364 (1)	0.650 (1)	0.188 (2)	9.2 (5)*
F(4a)	0.2059 (9)	0.6244 (8)	0.123 (2)	6.8 (3)*
F(1b)	0.250 (1)	0.743 (1)	0.073 (2)	11.3 (5)*
F(2b)	0.230 (1)	0.623 (1)	0.006 (2)	10.8 (4)*
F(3b)	0.368 (1)	0.646 (1)	0.130 (2)	7.4 (4)*
F(4b)	0.230 (2)	0.659 (2)	0.246 (3)	14.1 (6)*
C(33)	0.623 (3)	0.411 (2)	0.416 (5)	27 (2)*
C(32)	0.581 (2)	0.506 (2)	0.404 (4)	23 (1)*
C(31)	0.488 (2)	0.5460 (7)	0.486 (3)	15.9 (8)*
N(6)	0.926 (1)	0.125 (2)	0.220 (2)	20 (1)*
C(42)	0.868 (1)	0.209 (2)	0.241 (2)	14.5 (6)*
C(43)	0.807 (1)	0.240 (2)	0.358 (2)	28 (2)*
C(44)	0.803 (1)	0.188 (2)	0.453 (2)	16.6 (8)*
C(45)	0.860 (1)	0.104 (2)	0.432 (2)	18.8 (9)*
C(46)	0.922 (1)	0.073 (2)	0.316 (2)	25 (1)*

[a] Starred *B* values are for atoms that were refined isotropically. Anisotropically refined atoms are given in the form of the isotropic equivalent displacement parameter defined as $(4/3)[a^2B(1,1) + b^2B(2,2) + c^2B(3,3) + ab(\cos\gamma)B(1,2) + ac(\cos\beta)B(1,3) + bc(\cos\alpha)B(2,3)]$.

Table IV. Selected Bond Distances (Å) and Angles (deg) for $[\{Ru_2(chp)_4\}_2(pyz)](BF_4)_2\cdot 4CH_2Cl_2$[a]

Bond Distances			
Ru(1)–Ru(2)	2.2671 (7)	O(2)–C(21)	1.314 (8)
Ru(1)–O(1)	1.979 (4)	O(3)–C(31)	1.300 (8)
Ru(1)–O(2)	1.977 (4)	O(4)–C(41)	1.299 (7)
Ru(1)–O(3)	1.985 (4)	N(1)–C(11)	1.362 (8)
Ru(1)–O(4)	1.990 (4)	N(2)–C(21)	1.360 (8)
Ru(1)–N(5)	2.275 (5)	N(3)–C(31)	1.375 (8)
Ru(2)–N(1)	2.085 (5)	N(4)–C(41)	1.348 (9)
Ru(2)–N(2)	2.088 (5)	N(5)–C(1)	1.334 (8)
Ru(2)–N(3)	2.089 (5)	N(5)–C(2)	1.338 (8)
Ru(2)–N(4)	2.084 (5)	C(1)–C(2′)	1.369 (9)
O(1)–C(11)	1.328 (8)		

Bond Angles			
Ru(2)–Ru(1)–O(1)	90.9 (1)	N(1)–Ru(2)–N(4)	89.6 (2)
Ru(2)–Ru(1)–O(2)	91.1 (1)	N(2)–Ru(2)–N(3)	91.1 (2)
Ru(2)–Ru(1)–O(3)	91.1 (1)	N(2)–Ru(2)–N(4)	174.5 (2)
Ru(2)–Ru(1)–O(4)	91.1 (1)	N(3)–Ru(2)–N(4)	89.4 (2)
Ru(2)–Ru(1)–N(5)	179.3 (1)	Ru(1)–O(1)–C(11)	120.0 (4)
O(1)–Ru(1)–O(2)	89.6 (2)	Ru(1)–O(2)–C(21)	120.4 (4)
O(1)–Ru(1)–O(3)	177.9 (2)	Ru(1)–O(3)–C(31)	120.4 (4)
O(1)–Ru(1)–O(4)	90.0 (2)	Ru(1)–O(4)–C(41)	119.9 (4)
O(1)–Ru(1)–N(5)	89.0 (2)	Ru(2)–N(1)–C(11)	117.0 (4)
O(2)–Ru(1)–O(3)	91.0 (2)	Ru(2)–N(2)–C(21)	117.8 (4)
O(2)–Ru(1)–O(4)	177.8 (2)	Ru(2)–N(3)–C(31)	116.8 (4)
O(2)–Ru(1)–N(5)	88.2 (2)	Ru(2)–N(4)–C(41)	117.8 (4)
O(3)–Ru(1)–O(4)	89.3 (2)	Ru(1)–N(5)–C(1)	120.9 (4)
O(3)–Ru(1)–N(5)	88.9 (2)	Ru(1)–N(5)–C(2)	122.0 (4)
O(4)–Ru(1)–N(5)	89.6 (2)	C(1)–N(5)–C(2)	116.9 (5)
Ru(1)–Ru(2)–N(1)	88.2 (1)	N(5)–C(1)–C(2′)	121.6 (5)
Ru(1)–Ru(2)–N(2)	87.4 (1)	N(5)–C(2)–C(1′)	121.5 (6)
Ru(1)–Ru(2)–N(3)	87.7 (1)	O(1)–C(11)–N(1)	118.8 (6)
Ru(1)–Ru(2)–N(4)	87.2 (1)	O(2)–C(21)–N(2)	118.0 (5)
N(1)–Ru(2)–N(2)	89.4 (2)	O(3)–C(31)–N(3)	118.9 (6)
N(1)–Ru(2)–N(3)	175.8 (2)	O(4)–C(41)–N(4)	119.1 (5)

[a] Numbers in parentheses are estimated standard deviations in the least significant digits.

cell was determined via the indexing of 18 reflections in the 2θ range from 43 to 48°. The diffraction data were collected on an AFC5R Rigaku diffractometer equipped with Cu Kα radiation. There was an 8.1% overall decay during the period of data collection.

The approximate positions of the ruthenium atoms were derived from a Patterson map. The other non-hydrogen atoms were then introduced and refined as in the case of $[\{Ru_2(chp)_4\}_2(pyz)](BF_4)_2\cdot 4CH_2Cl_2$. A second set of partial fluorine atoms indicative of a disordered BF_4^- was found during the refinement of the molecule. The refinement with 50% occupancy for each set of fluorine atoms reached convergence. Free refinement of the pyridine molecule did not proceed well, and it was fixed as a regular hexagon. The crystallographic details are summarized in Table I, and the positional parameters are listed in Table III.

Results

Structure Descriptions. The cation for **1**, shown in Figure 1, consists of two diruthenium(II,III) tetrakis(μ-6-chloro-2-hydroxy)pyridinate units with a Ru–Ru distance of 2.267 (1) Å and one axially bridging pyz molecule with Ru(1)–N(pyz) distances of 2.275 (5) Å (Table IV). A crystallographic center of inversion is located at the midpoint of the bridging pyz molecule. The Ru(2)–Ru(1)–N(pyz) linkage is essentially linear. The nitrogen atom of pyrazine is attached to the ruthenium that is coordinated by four oxygen donor atoms of the chp ligands because the four chp ligands all point the same way, and the ruthenium coordinated by nitrogen atoms is sterically hindered by four chlorine atoms. The pyz molecule is strictly planar, and the pyz plane is only 8° away from being coplanar with the O(2)–Ru(1)–O(4)–C(41)–N(4)–Ru(2)–N(2)–C(21) plane.

The $[Ru_2(chp)_4(py)]^+$ cation is shown in Figure 2. The pyridine molecule is attached to the ruthenium atom that is coordinated by oxygen atoms. The Ru–Ru bond length is 2.2697 (8) Å with a Ru–N(py) distance of 2.205 (7) Å (Table V). The pyridine molecule is planar to within 0.01 Å, and the pyridine plane lies between the planes of the bridging chp groups with dihedral angles of 28.25 and 63.28° between pyridine and the O(1)–Ru(2)–O(3)–C(15)–N(3)–Ru(1)–N(1)–C(5) and O(2)–Ru(2)–O(4)–C(20)–N(4)–N(2)–C(10) planes, respectively.

Magnetic Properties. The magnetic susceptibilities of both compounds were measured from ca. 5 to ca. 300 K. The molar magnetic susceptibilities χ_M were calculated from the measured magnetic susceptibilities (χ_g), and molar diamagnetic corrections (χ_D) were also calculated on the basis of the Pascal constants. Magnetic moments and reciprocal magnetic susceptibility data for both $[\{Ru_2(chp)_4\}_2(pyz)](BF_4)_2$ and $[Ru_2(chp)_4(py)](BF_4)$ are shown as a function of temperature in Figure 3. The behavior of the two complexes is similar, and both compounds display

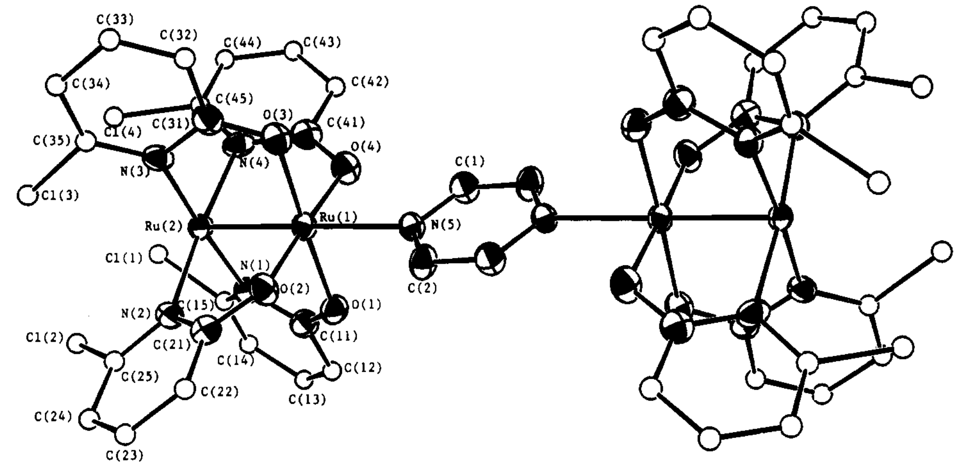

Figure 1. ORTEP drawing of $[\{Ru_2(chp)_4\}_2(pyz)]^+$ with 50% probability ellipsoids shown for all of the carbon atoms except the methine carbon and chlorine atoms. The molecule is located about an inversion center at the midpoint of the pyz molecule.

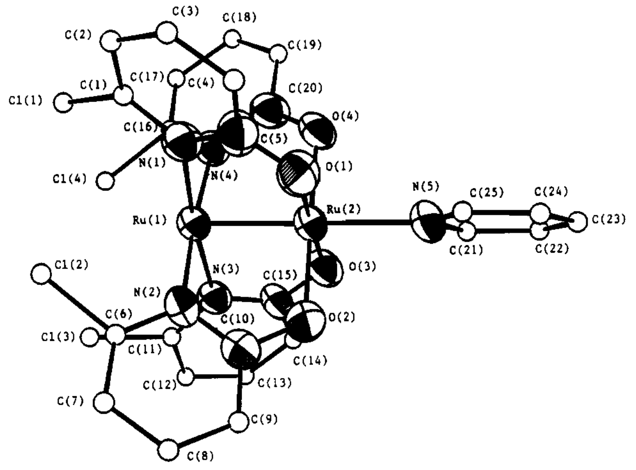

Figure 2. ORTEP drawing of $Ru_2(chp)_4(py)^+$ with 50% probability ellipsoids shown for all of the carbon atoms except the methine carbon and chlorine atoms.

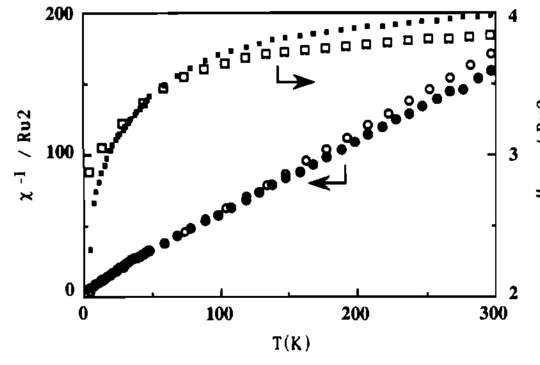

Figure 3. Magnetic moments per Ru_2 unit of $[\{Ru_2(chp)_4\}_2(pyz)](BF_4)_2$ (□) and $[Ru_2(chp)_4(py)](BF_4)$ (■) and reciprocal magnetic susceptibility data per Ru_2 unit of $[\{Ru_2(chp)_4\}_2(pyz)](BF_4)_2$ (○) and $[Ru_2(chp)_4(py)](BF_4)$ (●) as a function of temperature.

Table V. Selected Bond Distances (Å) and Angles (deg) for $[Ru_2(chp)_4(py)](BF_4)\cdot$hexane$\cdot$py[a]

	Bond Distances		
Ru(1)–Ru(2)	2.2697 (8)	O(1)–C(5)	1.30 (1)
Ru(1)–N(1)	2.107 (7)	O(2)–C(10)	1.34 (1)
Ru(1)–N(2)	2.060 (8)	O(3)–C(15)	1.313 (9)
Ru(1)–N(3)	2.092 (6)	O(4)–C(20)	1.31 (1)
Ru(1)–N(4)	2.077 (8)	N(1)–C(1)	1.34 (1)
Ru(2)–O(1)	1.976 (6)	N(1)–C(5)	1.37 (1)
Ru(2)–O(2)	1.963 (7)	N(2)–C(6)	1.38 (1)
Ru(2)–O(3)	1.980 (5)	N(2)–C(10)	1.35 (1)
Ru(2)–O(4)	1.991 (7)	N(3)–C(11)	1.35 (1)
Ru(2)–N(5)	2.205 (7)	N(3)–C(15)	1.35 (1)
Cl(1)–C(1)	1.742 (8)	N(4)–C(16)	1.34 (1)
Cl(2)–C(6)	1.734 (9)	N(4)–C(20)	1.37 (1)
Cl(3)–C(11)	1.735 (9)	N(5)–C(21)	1.33 (1)
Cl(4)–C(16)	1.72 (1)	N(5)–C(25)	1.36 (1)
	Bond Angles		
Ru(2)–Ru(1)–N(1)	87.2 (2)	O(3)–Ru(2)–O(4)	89.7 (3)
Ru(2)–Ru(1)–N(2)	87.6 (2)	O(3)–Ru(2)–N(5)	88.5 (2)
Ru(2)–Ru(1)–N(3)	86.9 (2)	O(4)–Ru(2)–N(5)	88.6 (3)
Ru(2)–Ru(1)–N(4)	88.1 (2)	Ru(2)–O(1)–C(5)	120.7 (5)
N(1)–Ru(1)–N(2)	91.5 (3)	Ru(2)–O(2)–C(10)	121.3 (5)
N(1)–Ru(1)–N(3)	174.1 (2)	Ru(2)–O(3)–C(15)	119.5 (5)
N(1)–Ru(1)–N(4)	89.0 (3)	Ru(2)–O(4)–C(20)	121.2 (6)
N(2)–Ru(1)–N(3)	88.5 (3)	Ru(1)–N(1)–C(1)	127.2 (5)
N(2)–Ru(1)–N(4)	175.7 (2)	Ru(1)–N(1)–C(5)	116.5 (5)
N(3)–Ru(1)–N(4)	90.6 (3)	C(1)–N(1)–C(5)	116.3 (7)
Ru(1)–Ru(2)–O(1)	91.0 (2)	Ru(1)–N(2)–C(6)	126.5 (6)
Ru(1)–Ru(2)–O(2)	90.5 (2)	Ru(1)–N(2)–C(10)	118.4 (6)
Ru(1)–Ru(2)–O(3)	91.2 (1)	C(6)–N(2)–C(10)	114.5 (9)
Ru(1)–Ru(2)–O(4)	90.4 (2)	Ru(1)–N(3)–C(11)	126.4 (5)
Ru(1)–Ru(2)–N(5)	179.1 (2)	Ru(1)–N(3)–C(15)	117.7 (5)
O(1)–Ru(2)–O(2)	91.0 (3)	C(11)–N(3)–C(15)	115.9 (7)
O(1)–Ru(2)–O(3)	177.8 (2)	Ru(1)–N(4)–C(16)	125.6 (7)
O(1)–Ru(2)–O(4)	90.3 (3)	Ru(1)–N(4)–C(20)	116.9 (5)
O(1)–Ru(2)–N(5)	89.3 (2)	C(16)–N(4)–C(20)	117.0 (9)
O(2)–Ru(2)–O(3)	88.9 (3)	Ru(2)–N(5)–C(21)	121.0 (6)
O(2)–Ru(2)–O(4)	178.4 (2)	Ru(2)–N(5)–C(25)	121.1 (7)
O(2)–Ru(2)–N(5)	90.4 (3)	C(21)–N(5)–C(25)	117.9 (8)

[a] Numbers in parentheses are estimated standard deviations in the least significant digits.

Curie–Weiss behavior. The decrease in moment at low temperatures results primarily from zero-field splitting effects. The close similarity of these plots indicates a lack of any noteworthy magnetic exchange interactions between two dinuclear species in $[\{Ru_2(chp)_4\}_2(pyz)](BF_4)_2$. The magnetic moment per dinuclear unit in $[\{Ru_2(chp)_4\}_2(pyz)](BF_4)_2$ is 3.99 μ_B, while that of $[Ru_2(chp)_4(py)](BF_4)$ is 3.87 μ_B at room temperature.

Discussion

The results obtained pretty well speak for themselves. As far as the first objective stated in the Introduction, we have succeeded. Both the pyrazine-bridged species, $[\{Ru_2(chp)_4\}_2(pyz)]^{2+}$, and a suitable species for comparison, namely $[Ru_2(chp)_4(py)]^+$, have been prepared and structurally characterized. The $Ru_2(chp)_4$ portions of each one are virtually identical. The attachment of the aromatic base does differ slightly from one case to the other in two respects. In the pyrazine case the plane of the aromatic base nearly coincides with two of the ligand planes of the $Ru_2(chp)_4$ units whereas in $[Ru_2(chp)_4(py)]^+$ the pyridine ring plane is nearly staggered with respect to the ligand planes. There is also a slight difference in the Ru–N distances, with that to pyridine being ca. 0.06 Å shorter. This could help to account for the very slight differences in the magnetic properties of the two compounds.

It is quite clear that the bridging pyrazine ligand has in this case proved to be ineffective in coupling the magnetic moments of the two $Ru_2(chp)_4^+$ ions. We are somewhat surprised and disappointed by this. In view of the fact that the $Ru_2(chp)_4^+$ unit has two of its three unpaired electrons present in π^* orbitals, we had hoped that, by overlap of these with the π or π^* orbitals of the pyrazine ring, significant interaction would be facilitated.

Acknowledgment. We thank the National Science Foundation for support and Professor Tobin Marks and Douglas Schulz of Northwestern University for the magnetic measurements.

Supplementary Material Available: Tables of anisotropic thermal parameters, bond length and angle data, and least-squares planes for $1{\cdot}4CH_2Cl_2$ and **2**, tables of crystal data, atomic positional parameters, anisotropic thermal parameters, bond length and angle data, and least-squares planes and an ORTEP diagram for $1{\cdot}2CH_2Cl_2{\cdot}2pyz$, figures showing IR spectra of **1** and **2**, and tables of variable-temperature magnetic susceptibility data for **1** and **2** (30 pages); listings of observed and calculated structure factors for $1{\cdot}4CH_2Cl_2$, $1{\cdot}2CH_2Cl_2{\cdot}2pyz$, and **2** (73 pages). Ordering information is given on any current masthead page.

Contribution from the Department of Chemistry and Center for Molecular Electronics,
Center for Science and Technology, Syracuse University, Syracuse, New York 13244-4100

Small Heteroborane Cluster Systems. 5. Factors Affecting the 2D ^{11}B–^{11}B COSY NMR Spectra of Terminal- and Bridge-Substituted Pentaborane Cluster Systems[1]

Bruce H. Goodreau and James T. Spencer*

Received August 8, 1991

The ^{11}B–^{11}B correlation NMR spectra (2D ^{11}B–^{11}B COSY NMR) and T_1 relaxation times for pentaborane(9), B_5H_9, and 10 terminal- and bridge-substituted pentaborane clusters, including phosphinopentaboranes, silylpentaboranes, and metal pentaborane complexes, have been measured. Both J_{PB} and "long-range" $^2J_{PBB}$ couplings, observed the first time in boranes, were measured for the (μ-phosphino)pentaborane compounds. The long-range $^2J_{PBB}$ couplings were not directly observable in the normal 1D spectra but were clearly resolved in the cross peaks of the 2D spectra. The magnitudes of these J_{PB} and $^2J_{PBB}$ coupling constants were related to the calculated MO cage bonding scheme for the clusters. A direct relationship between the MNDO-calculated boron–boron bond orders and the intensity of the developed cross peaks in the 2D ^{11}B–^{11}B COSY NMR spectra for adjacent cage boron atoms was observed which relates the calculated electron density localized in bonding interactions to observed NMR parameters in the clusters. The relationship among the MNDO-calculated bond order, T_1 relaxation time, and the appearance of cross peaks in COSY spectra has been evaluated. The first double-quantum ^{11}B–^{11}B correlation NMR experiment for the framework cage elucidation of a borane cluster is reported.

Introduction

Since 1982 homonuclear ^{11}B–^{11}B correlation NMR (^{11}B–^{11}B COSY NMR) spectroscopy has been widely used for the elucidation of the structural features and the assignment of NMR spectral resonances for new boron cluster compounds.[2] Since then, the technique has been extended to include other quadrupolar nuclei such as ^{51}V ($I = {}^7/_2$).[3] Over the last 9 years, however, relatively little has been done to quantify the parameters associated with the development of a cross peak between coupled boron atoms.[2,4]

In the 2D NMR experiment, cross peaks (off-diagonal peaks) reveal spin–spin coupling interactions between the correlated nuclei.[5,6] In ^{11}B–^{11}B homonuclear COSY NMR spectra, the presence or absence of these cross peaks has been used effectively in the assignment of framework connectivities in unknown cage structures.[2] The systematic absence of a cross peak where one would normally be expected to develop has caused, in some cases, significant assignment difficulties, resulting in structural ambiguity for these new cages. This problem has been especially pronounced for the heteroborane and metallaborane clusters. It is therefore of importance to address the underlying chemical reasons for cross peak absences in 2D ^{11}B–^{11}B NMR spectra in order to improve the applicability of this powerful method toward making reliable cage framework assignments.

The two most important factors governing cross peak evolution in the 2D spectrum are the amount of electron density localized between the boron atoms in question and the relaxation times for these nuclei.[2b,5,6] In this paper, we address these parameters quantitatively by calculating boron–boron bond orders using semiempirical theoretical techniques and by measuring the 2D spectra and T_1 values for the cage boron atoms in a variety of substituted pentaborane cluster compounds. Since the presence of a cross peak in the 2D experiment requires the localization of significant electron density between correlated nuclei, because scalar coupling is propagated primarily through the bonding electrons, it should be possible to obtain a correlation between the calculated boron–boron bond order and the development of a cross peak in the 2D spectrum, assuming that the corresponding T_1 values are sufficiently long. This expectation is supported by the qualitative relationship observed between the expected bonding

---

* To whom correspondence should be addressed at the Department of Chemistry.

(1) Part 4: Goodreau, B. H.; Orlando, L. R.; Spencer, J. T. *J. Am. Chem. Soc.*, in press.

(2) (a) Venable, T. L.; Hutton, W. C.; Grimes, R. N. *J. Am. Chem. Soc.* **1982**, *104*, 4716. (b) Venable, T. L.; Hutton, W. C.; Grimes, R. N. *J. Am. Chem. Soc.* **1984**, *106*, 29. (c) Wang, Z.; Sinn, E.; Grimes, R. N. *Inorg. Chem.* **1985**, *24*, 826. (d) Brewer, C. T.; Grimes, R. N. *J. Am. Chem. Soc.* **1985**, *107*, 3552. (e) Brewer, C. T.; Swisher, R. G.; Sinn, E.; Grimes, R. N. *J. Am. Chem. Soc.* **1985**, *107*, 3558. (f) Gaines, D. F.; Edvenson, G. M.; Hill, T. G.; Adams, B. R. *Inorg. Chem.* **1987**, *26*, 1813. (g) Edvenson, G. M.; Gaines, D. F.; Harris, H. A.; Campana, C. F. *Organometallics* **1990**, *9*, 410. (h) Meina, D. G.; Morris, J. H.; Reed, D. *Polyhedron* **1986**, *5*, 1639. (i) Jacobsen, G. B.; Meina, D. G.; Morris, J. H.; Thomson, C.; Andrews, S. J.; Reed, D.; Welch, A. J.; Gaines, D. F. *J. Am. Chem. Soc., Dalton Trans.* **1985**, 1645. (j) Fontaine, X. L. R.; Greenwood, N. N.; Kennedy, J. D.; MacKinnon, P. *J. Chem. Soc., Dalton Trans.* **1988**, 1785. (k) Howarth, O. W.; Jasztal, M. J.; Taylor, J. G.; Wallbridge, M. G. H. *Polyhedron* **1985**, *4*, 1461. (l) Hermanek, S.; Fusek, J.; Stibr, B.; Plesek, J.; Jelinek, T. *Polyhedron* **1986**, *5*, 1873. (m) Jelinek, T.; Stibr, B.; Mares, F.; Plesek, J.; Hemanek, S. *Polyhedron* **1987**, *6*, 1737. (n) Kester, J. G.; Huffman, J. C.; Todd, L. J. *Inorg. Chem.* **1988**, *27*, 4528. (o) Kang, S. O.; Carroll, P. J.; Sneddon, L. G. *Organometallics* **1988**, *7*, 772. (p) Little, J. L.; Whitesell, M. A.; Kester, J. G.; Folting, K.; Todd, L. J. *Inorg. Chem.* **1990**, *29*, 804. (q) Getman, T. D.; Deng, H.-B.; Hsu, L.-Y.; Shore, S. G. *Inorg. Chem.* **1989**, *28*, 3612.

(3) Sanders, J. K.; Hunter, B. K. *Modern NMR Spectroscopy*; Oxford University Press: Oxford, U.K., 1988.

(4) Khan, S. A.; Morris, J. H.; Siddiqui, S. *J. Chem. Soc., Dalton Trans.* **1990**, 2053.

(5) Bax, A. *Two Dimensional Nuclear Magnetic Resonance in Liquids*; Delft University Press: Dordrecht, Holland, 1982.

(6) (a) Schraml, J.; Bellama, J. M. *Two-Dimensional NMR Spectroscopy*; Wiley: New York, 1988. (b) Drago, R. S. *Physical Methods in Chemistry*; Saunders: Philadelphia, PA, 1977.

0020-1669/92/1331-2612$03.00/0